The Journal of Experimental Biology 213, 2184-2193

doi:10.1242/jeb.040972

Snout allometry in seahorses: insights on optimisation of pivot feeding performance during ontogeny

Gert Roos[1,*], Sam Van Wassenbergh[1], Anthony Herrel[1,2], Dominique Adriaens[3] and Peter Aerts[1,4]

[1]Department of Biology, Universiteit Antwerpen, Universiteitsplein 1, B-2610 Antwerpen, Belgium, [2]Département d'Ecologie et de Gestion de la Biodiversité, Muséum National d'Histoire Naturelle, 57 rue Cuvier, Case postale 55, 75231, Paris Cedex 5, France, [3]Evolutionary Morphology of Vertebrates, Ghent University, K.L. Ledeganckstraat 35, B-9000 Gent, Belgium and [4]Department of Movement and Sports Sciences, Ghent University, Watersportlaan 2, B-9000 Gent, Belgium

*Author for correspondence (gert.roos@ua.bc.be)

Accepted 17 March 2010

SUMMARY

As juvenile life-history stages are subjected to strong selection, these stages often show levels of performance approaching those of adults, or show a disproportionately rapid increase of performance with age. Although testing performance capacity in aquatic suction feeders is often problematic, in pivot feeders such as seahorses models have been proposed to estimate whether snout length is optimal to minimise the time needed to reach the prey. Here, we investigate whether the same model can also explain the snout lengths in an ontogenetic series of seahorses, explore how pivot feeding kinematics change during ontogeny, and test whether juveniles show disproportionate levels of performance. Our analysis shows that the dimensions of the snout change during ontogeny from short and broad to long and narrow. Model calculations show that the snout lengths of newborn and juvenile seahorses are nearly optimal for minimising prey reach time. However, in juveniles the centre of head rotation in the earth-bound frame of reference is located near the posterior end of the head, whereas in adults it is shifted forward and is located approximately above the eye. Modelling shows that this forward shift in the centre of rotation has the advantage of decreasing the moment of inertia and the torque required to rotate the head, but has the disadvantage of slightly increasing the time needed to reach the prey. Thus, the snout lengths of juvenile seahorses appear to be close to optimal, suggesting that they reach levels of performance close to adult levels, which illustrates the pervasive nature of selection on performance in juveniles.

Key words: Syngnathidae, pivot feeding, ontogeny, scaling.

INTRODUCTION

As juvenile life-history stages are subjected to strong selection (Carrier, 1996; Herrel and Gibb, 2006), these stages often show levels of performance approaching those of adults, or show a disproportionately rapid increase of performance with age (Carrier, 1995; Herrel and O'Reilly, 2006; Moon and Tullis, 2006). Although there is considerable empirical support for this paradigm in terrestrial organisms (for a review, see Herrel and Gibb, 2006) it is currently unclear whether it also applies in aquatic environments for traits other than escape performance (Gibb et al., 2006). However, testing performance capacity in aquatic suction feeders is often problematic (Holzman et al., 2008). However, in pivot feeders, such as seahorses, models have been proposed to estimate performance, which is defined as the ability to minimise the time needed for the mouth to reach the prey by rotating the head (de Lussanet and Muller, 2007). Indeed, a critical aspect of aquatic suction feeding is to bring the mouth close enough to the prey, so that the prey can effectively be drawn into the mouth by the suction flow generated (Holzman et al., 2007; Wainwright and Day, 2007; Holzman et al., 2008). Consequently, this model could be used to test whether one aspect of suction feeding is optimised in juvenile life-history stages in pivot-feeding fishes.

Pivot feeders, like syngnathids (Muller, 1987; Bergert and Wainwright, 1997; Colson et al., 1998; de Lussanet and Muller, 2007; Van Wassenbergh et al., 2008; Roos et al., 2009a), flatfish (Muller and Osse, 1984; Gibb, 1997) and presumably viperfish (Tchernavin, 1953; Muller, 1987) do not rotate the neurocranium to increase the mouth opening (as in typical suction feeders), but rotate their head to decrease the mouth–prey distance. When head rotation reaches its maximum (and the mouth opening is directed towards the prey), the buccal cavity starts to expand and draws the prey into the mouth (Roos et al., 2009b). During pivot feeding only the head of the fish is accelerated towards the prey, while the body remains approximately stationary (Van Wassenbergh et al., 2008). This is probably energetically more advantageous than swimming towards the prey. Moreover, studies of syngnathid pivot feeding have reported relatively large lift angles of the head during feeding, for example 30 deg in *Syngnathus acus* (de Lussanet and Muller, 2007), 25 deg in *Syngnathus leptorhynchus* (Van Wassenbergh et al., 2008) and 25 deg in *Hippocampus reidi* (Roos et al., 2009a). Particularly in fish with elongated heads, such lift angles allow the mouth to overcome greater distances than could be possible by jaw protrusion alone.

Among syngnathid pivot feeders, a large interspecific variation in snout dimensions exists between adults. Snouts vary from extremely elongated and narrow, as observed in for example the weedy seadragon *Phyllopteryx taeniolatus* (Forsgren and Lowe, 2006; Kendrick and Hyndes, 2005), to very stout and broad, for example the pygmy seahorse *Hippocampus denise* (Lourie and Randall, 2003). Given this variation in head and snout dimensions the question arises of how this affects pivot feeding. A recent theoretical model by de Lussanet and Muller (de Lussanet and Muller, 2007) predicted the optimal snout length in syngnathids for reaching the prey as quickly as possible by rotation of head and

snout. This study showed that species with longer snouts generally have a smaller cross-sectional diameter of the snout, which (at least partly) compensates for the increased moment of inertia resulting from their relatively high snout length. Because of a similar moment of inertia and narrower snouts, the species with relatively long snouts will reach their prey faster than species with relatively short snouts. This theoretical model was confirmed by anatomical measurements in a wide range of syngnathid species (de Lussanet and Muller, 2007).

However, not only in an evolutionary, interspecific context, but also during ontogeny, the snout of syngnathids undergoes significant morphological changes (Choo and Liew, 2006; Leysen et al., 2010). Choo and Liew (Choo and Liew, 2006) showed that the shape of the snout changes significantly throughout ontogeny in *Hippocampus kuda*. For example, after the juveniles are expelled from the male's brood pouch, the head length is 25–33% of the standard length (the summation of head, trunk and tail length), but this proportion decreases sharply to 17% for 3-week-old juveniles. The study of Choo and Liew (Choo and Liew, 2006) only addressed scaling of morphological traits such as head, trunk and tail length (Lourie et al., 1999) relative to standard length, yet, their illustrations of different ontogenetic stages of seahorses suggest that the shape and size of different head parts also change. This could affect the kinematics of pivot feeding during the first few weeks after the juveniles are expelled from the brood pouch.

Given this apparent cranial allometry in seahorses (Choo and Liew, 2006; Leysen et al., 2010) it can be questioned whether the previously documented snout-length optimisation principles (de Lussanet and Muller, 2007) also apply to growing seahorses. At first glance, important kinematic differences seem to exist between adults and newborns. Van Wassenbergh et al. (Van Wassenbergh et al., 2009) showed that newly born seahorses of the species *Hippocampus reidi* only need 2.5 ms to rotate their head over 40 deg. Adults, by contrast, need twice the time to rotate their head over merely 25 deg (Roos et al., 2009a). However, the form–function relationships of the pivot feeding system in this ontogenetic series of seahorse remain unclear.

In this paper, we examine whether snout length is indeed optimised for pivot feeding in juvenile compared with adult life history stages in the seahorse *H. reidi*. The ontogenetic series consists of four juvenile age classes during which important morphological changes occur (less than 1 week, 1 week, 2 weeks and 3 weeks) (Choo and Liew, 2006), and adults. To test this hypothesis and to quantify an important aspect of suction feeding performance the model of de Lussanet and Muller (de Lussanet and Muller, 2007) is used. To generate the required input data for the model a kinematical analysis (high-speed video analysis) was used, allowing us to determine the position of the centre of rotation in the earth-bound frame of reference. Morphometric data, in turn, allowed us to estimate the moment of inertia of the head and snout in each age class. Finally, scaling analyses were used to evaluate whether the measured dimensions of head and snout relevant for pivot feeding change during ontogeny.

MATERIALS AND METHODS

Husbandry

A total of 15 adult individuals of the seahorse species *Hippocampus reidi* Ginsburg 1933 were obtained through the commercial aquarium trade. These seahorses were kept together in a large tank (600 l) with a constant temperature of 24°C and constant salinity of 35 p.p.t. Animals were fed defrosted mysids daily. When a male seahorse expressed signs of pregnancy, it was placed inside a large net in the same tank and was left undisturbed. As the juveniles left the male's pouch, they were captured in the net and were transferred to a smaller tank (30 l). These juveniles were fed freshly hatched brine shrimps, three times a day. Several males gave birth at different times and batches of different ages were kept in separate tanks. In total, five different age classes were used in this study: less than 1 week, 1, 2 and 3 weeks, and adults.

Scaling of head and snout dimensions

A total of 76 specimens (20, 20, 11, 15 and 10 individuals for each of the age classes, respectively, with standard lengths (± s.d.) of 5.83±0.43, 7.11±0.77, 10.12±1.50, 12.57±1.52 and 106.66±6.94 mm, respectively) were photographed using an ALTRA 20 camera (resolution 1596×1196 pixels; Soft Imaging System GmbH, Münster, Germany) in lateral and in dorsal view. Specimens were preserved in neutralised and buffered formalin solution for 5 months. The head and snout dimensions in each digital photo were measured using ImageJ software (version 1.41m, W. Rasband, National Institute of Mental Health, Bethesda, MA, USA). In analogy with de Lussanet and Muller (de Lussanet and Muller, 2007), snout shape was approximated by an elliptical cylinder and the head without the snout was modelled as a half-ellipsoid (Fig. 1). The snout length (l) was measured as the distance between the point at the level of the neck joint (the intercept of the line starting from the middle of the coronet to the dorsal ridge of the operculum) to the tip of the snout. The snout width (w) was measured at the level of the articulation of the lower jaw with the quadrate, and the snout height (h) was measured from the articulation of the lower jaw with the quadrate to the frontal tip of the vomer. The head length (L) was measured as the distance between the point at the level of the neck joint and the anterior part of the frontal bone. The head height (H) was determined perpendicular to L at the level of the approximate neck joint, and head width (W) was the distance between the opercula (Fig. 1).

Morphometric data were log-transformed and regressed on snout length. The slopes of the regression lines were determined for each plot. To test whether each slope was significantly different from the predicted slope (isometry, slope=1), the latter was subtracted from the measured slope and divided by the standard error of the measured slope (s.e.m.) to obtain a t-value (Sokal and Rohlf, 1995). Slopes significantly smaller than 1 indicate negative allometry, whereas a slope greater than 1 indicates positive allometry.

High-speed video recordings

During filming sessions, the juveniles were transferred to a very small glass tank (6 ml). Several juveniles (two or three) were placed in this tank and multiple prey items were provided to increase the chance of capturing a feeding event on video. The duration of a filming session was 30 min after which the juveniles were replaced by two or three other juveniles. Adults were transferred to a 30 l tank, with a narrow section. The adult seahorses were trained to feed in this section to increase the chance of filming the animals with the midsagittal plane of their heads at an angle perpendicular to the camera.

Videos were made with a digital high-speed video camera (Redlake Motionscope M3, Redlake Inc., Tallahassee, FL, USA) with a 20 mm lens (Sigma EX, Sigma Benelux, Nieuwegein, The Netherlands). Two arrays of eight ultra bright LEDs were used for illumination. The videos of the juveniles and the adults were recorded at a speed of 8000 frames per second and a shutter time of 0.05 ms. Only videos with the side of the head oriented perpendicular to the camera lens were retained for further analysis.

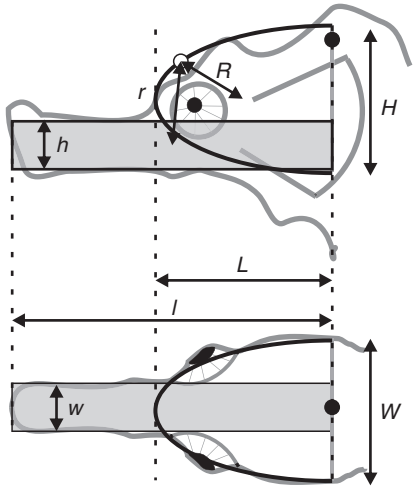

Fig. 1. In analogy with the model of de Lussanet and Muller (de Lussanet and Muller, 2007), the snout, and the head without the snout are approximated by an elliptic cylinder and by a half-ellipsoid, respectively. The filled circle indicates the position of the neck joint and the open circle approximates the position of the centre of rotation. With *H*, *L* and *W* the height, length and width, respectively, of the head, and *h*, *l* and *w* the height, length and width, respectively, of the snout. The parameters *R* and *r* indicate the distance of the centre of rotation and the middle of the head and the snout, respectively. According to de Lussanet and Muller (de Lussanet and Muller, 2007), the difference between model output with or without the snout continuing within the head base was negligible. Therefore, this simplification was also used in this study.

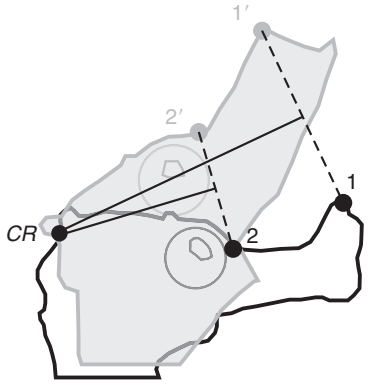

Fig. 2. Schematic illustration of the position of the two digitised landmarks (1, 2) used to measure head rotation from the video recordings. The same landmarks were used to determine the position of the centre of head rotation (*CR*; for further explanation see text). The position of the seahorse head at the beginning of the feeding strike is indicated by the black outline and the two landmarks being 1 and 2. The position of the seahorse head near maximal head rotation is indicated by the grey image with the position of the respective landmarks at that time represented by 1′ and 2′.

A total of 71 videos were analysed: 11, 16, 14, 18 and 12 for the age classes of, less than 1, 1, 2, 3 weeks and adult, respectively. Four recordings were analysed for each of the three adult individuals. The juveniles, however, could not be distinguished from one another during filming sessions. To avoid pseudoreplication, the juvenile data was averaged for individuals filmed in the same tank during a filming session (Hernandez, 2000).

Centre of head rotation

The position of the centre of rotation (*CR*) was calculated based on the high-speed video recordings for each age class (Van Wassenbergh et al., 2008). To simplify the estimation of the position of *CR*, the head and body were treated as two rigid elements and the average position of the *CR* was calculated for a pre-defined time interval. A fixed time interval was selected for each of the 71 video recordings from the beginning of the feeding strike (i.e. prior to the start of hyoid rotation and thus prior to head rotation, time=0 ms) until the frame at which the head rotation was near its maximum (time=2 ms and 3 ms for juveniles and adults, respectively). Two landmarks were traced in each of these frames: the tip of the snout and the tip of the nose spine just anterior to the eye. The common centre of the angular displacement of these two landmarks (i.e. the *CR*) was determined as the intersection of the mid-normals of the line segments interconnecting each landmark at the start and end of the time interval (Fig. 2). As the velocity of the seahorse from swimming during this short time interval is negligibly small (only $0.02\,\mathrm{m\,s^{-1}}$), this common centre corresponds to *CR* in the earth-bound frame of reference (de Lussanet and Muller, 2007; Van Wassenbergh et al., 2008).

Next, the distance *R* between *CR* and the centre of volume of the head (approximated by a half-ellipsoid) and the distance *r* between *CR* and the middle of the snout volume (approximated by an elliptical cylinder) were calculated for each age class (Fig. 1). *R* and *r* were log-transformed and regressed to log snout length (*l*). Like the analysis of the morphometric data, the slopes of the regression lines were calculated and tested for isometry as described above.

Moment of inertia

First, the model of de Lussanet and Muller (de Lussanet and Muller, 2007) requires the moment of inertia of head and snout as input. Since the dimensions of head and snout and the position of *CR* are determined, the moment of inertia of head and snout relative to this defined *CR* can be calculated as follows (de Lussanet and Muller, 2007):

$$I_{\mathrm{head}} = \alpha_{\mathrm{head}} \frac{\rho\pi WHL}{6}\left(\left(\frac{1}{5}-\frac{9}{64}\right)L^2+\frac{H^2}{20}+R^2\right), \quad (1)$$

$$I_{\mathrm{snout}} = \alpha_{\mathrm{snout}} \frac{\rho\pi whl}{4}\left(\frac{l^2}{12}+\frac{h^2}{16}+r^2\right), \quad (2)$$

where *W*, *H*, *L* are the width, height and length, respectively, of the half-ellipsoid (the head) and *w*, *h*, *l* are the width, height and length, respectively, of the elliptical cylinder (the snout). The density ρ is the density of the surrounding seawater, which is $1023\,\mathrm{kg\,m^{-3}}$. When the head rotates in the water column, unavoidably an amount of water around the head and snout will be accelerated as well. To account for this added mass of water, we calculated a correction factor for head (α_{head}) and snout (α_{snout}) using the added mass coefficients of flow over elliptical cylinders with different aspect ratios with the formula given in Van Wassenbergh et al. (Van Wassenbergh et al., 2008) which is derived from Daniel (Daniel, 1984):

$$\alpha_{\mathrm{head}} = 2.1438^{-0.784H/W}+1 \quad (3)$$

$$\alpha_{\mathrm{snout}} = 2.1438^{-0.784h/w}+1\,. \quad (4)$$

The moment of inertia of head and snout with respect to *CR* was calculated for each individual of each age class. The total moment of inertia I_{total} relative to *CR* was the sum of I_{head} and I_{snout} (de

Lussanet and Muller, 2007). Note that de Lussanet and Muller (de Lussanet and Muller, 2007) did not include the terms r and R in their presented formulas although the terms were included in their actual simulations. Here, we worked out the same formulas but with inclusion of the R and r terms:

$$I_{\text{total}} = I_{\text{head}} + I_{\text{snout}}$$

$$I_{\text{total}} = I_{\text{head}} + \alpha_{\text{snout}}\rho\pi whl\left(\frac{l^2}{48}+\frac{h^2}{64}+\frac{r^2}{4}\right)$$

$$I_{\text{total}} = I_{\text{head}} + \alpha_{\text{snout}}\rho\pi\left(\frac{whl^3}{48}+\frac{wh^3l}{64}+\frac{whlr^2}{4}\right). \quad (5)$$

To estimate the accuracy of I_{total} obtained from the two simple geometric figures, we also calculated I_{total} using the method described in Drost and van den Boogaart (Drost and van den Boogaart, 1986). In this method the head was represented as a series of elliptical cylinders and I_{total} was the sum of the moment of inertia of each cylinder relative to *CR* (see also Van Wassenbergh et al., 2008). In this way, I_{total} could be calculated more precisely, accounting for contour lines of the head and snout. The difference between I_{total} obtained from the two geometric figures and I_{total} obtained from 20 elliptical cylinders was less than 10%. To keep the model as simple as possible, we chose the method in which the head and snout are represented by a half-ellipsoid and an elliptical cylinder, respectively.

For the scaling analysis, this data was log-transformed and regressed to log snout length (l). The slope of the regression line was determined, and a t-test, as described above, was used to test for isometry (slope=5).

Work input

A second model input that is required is a realistic amount of work done by the head elevator muscles in generating head rotation (de Lussanet and Muller, 2007). The angular velocity, needed to calculate the rotational kinetic energy was obtained from the high-speed video recordings.

In the 71 selected videos, the same two landmarks, used to determine the centre of head rotation, were digitised frame by frame using Didge (version 2.2.0, A. Cullum, Creighton, Omaha, NE, USA) (Fig. 2). With these two landmarks, head rotation was calculated. The profiles were filtered with a fourth-order, zero phase-shift Butterworth filter with a low-pass cut-off frequency of 2000 Hz to reduce digitisation noise. Angular velocity of head rotation was obtained through numerical differentiation. The maximum head rotation, the angular velocity of head rotation, the time to peak head rotation and angular velocity were log-transformed and regressed to log snout length. Finally, to study kinematic scaling relationships, the slopes of the regression lines were calculated. These analyses were performed for the adult and juvenile data combined and for the juvenile data with exclusion of the adult data. In this way we could investigate whether the kinematic scaling relationship is a result of changes in morphological structures or because of the large size difference between adults and juveniles.

Now the rotational kinetic energy E, needed to rotate the head can be calculated with the formula:

$$E = \frac{I_{\text{total}}\bar{\theta}_T^2}{2}, \quad (6)$$

where I_{total} is the total moment of inertia of head and snout relative to *CR* (Eqn 5) and $\bar{\theta}_T$ is the average maximal angular velocity of head rotation obtained from the high-speed videos.

Minimal reach time and optimal snout length

The angle θ_T over which the head needs to rotate for the mouth to travel distance d to reach the prey is:

$$\theta_T = \arcsin\left(\frac{d}{f}\right), \quad (7)$$

which was approximated by:

$$\theta_T \approx \left(\frac{d}{f}\right), \quad (8)$$

in which f is the distance between *CR* and the tip of the snout. The variables d and f were measured and adjusted for each age class to account for a possible change of prey position relative to the snout tip during ontogeny. For the largest head rotation observed in our data (44 deg), we numerically validated that the simplifying approximation of Eqn 7 did not significantly affect the outcome of the model (i.e. optimum snout length). A combination of Eqns 6, 7 and 9 gives (de Lussanet and Muller, 2007):

$$t = \frac{\theta_T}{\bar{\theta}_T} \approx \frac{d}{f}\sqrt{\frac{I_{\text{total}}}{2E}}. \quad (9)$$

When we substitute Eqn 5 into Eqn 9, we can calculate the reach time for a given snout length:

$$t \approx \sqrt{\frac{\alpha_{\text{snout}}\rho\pi d^2}{2Ef^2}\left(\frac{I_{\text{head}}}{\alpha_{\text{snout}}\rho\pi}+\frac{whl^3}{3}+\frac{wh^3l}{4}+\frac{whlr^2}{4}\right)}. \quad (10)$$

The minimal reach time can be found by solving Eqn 10 for a continuous range of snout lengths. In this way the optimal snout length l_{opt}, which corresponds to the minimal reach time t_{min}, can be determined.

Paired t-tests were used to statistically compare the measured snout lengths with the calculated optimal snout lengths, predicted by the model, for different individuals of each age class.

Effect on the position of the centre of rotation on the optimal snout length

de Lussanet and Muller (de Lussanet and Muller, 2007) calculated the optimal snout length for several syngnathid representatives

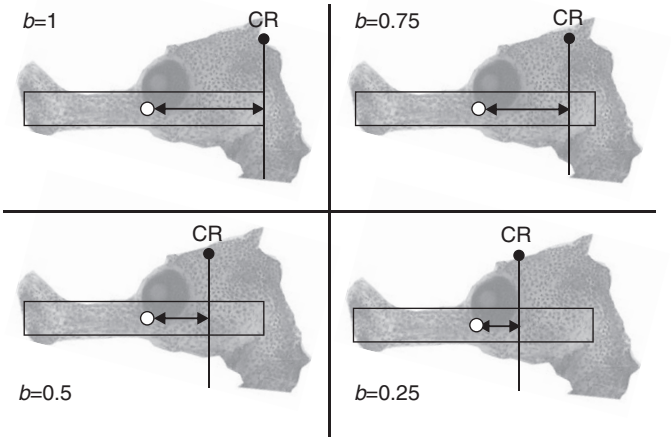

Fig. 3. Examples of the different position of the centre of head rotation (*CR*). The elliptical cylinder represents the snout (see Fig. 1) and the white circle indicates the middle of the volume. The arrows indicate different lengths of *b*, which is the perpendicular distance between the middle of the snout volume and the vertical line through the *CR*. The four discrete positions of *b* are in clockwise direction *b*, 0.75*b*, 0.5*b* and 0.25*b*.

Table 1. Results of the linear regression analysis on the log–log-transformed dimensions of head and snout relative to snout length

Variable	*N*	Slope	s.e.m.	R^2	Isometric slope	*P**
Snout width	76	0.88	0.01	0.99	1	<0.0001
Snout height	76	0.90	0.01	0.99	1	<0.0001
Head length	76	0.89	0.01	0.99	1	<0.0001
Head width	76	0.66	0.01	0.99	1	<0.0001
Head height	76	0.92	0.01	0.99	1	<0.0001
R	62	0.89	0.01	0.99	1	<0.0001
r	62	0.67	0.01	0.99	1	<0.0001
I	76	4.53	0.02	0.99	1	<0.0001

The parameters *R*, *r*, *I* represents the distance of the centre of rotation to the middle of the head volume, the distance of the centre of rotation to the middle of the snout volume and the total moment of inertia with respect to the centre of rotation, respectively.

**P*-value is the result of a *t*-value which was obtained by subtracting the measured slope with the predicted (isometric) slope, divided by s.e.m. of the measured slope.

assuming the position of the centre of rotation (*CR*) in each species is equal to the position of *CR* in *Syngnathus acus*. Given that the juveniles of *Hippocampus kuda* undergo morphological changes during growth (Choo and Liew, 2006), it can be expected that the position of *CR* will change in the different age classes of *Hippocampus reidi* used in this study. We used the model of de Lussanet and Muller (de Lussanet and Muller, 2007) to investigate how the change in position of *CR* affects the optimal snout length.

We assumed that the position of *CR* could change relative to its *in vivo CR* by translating parallel to the snout length axis. We defined *b* as the distance between *CR* and the midpoint of the snout along the snout length axis divided by the distance between the most posterior point on the head and *CR* along the same axis (Fig. 3). For practical reasons, we used four discrete values of *b* in each age class: *b*=1, *b*=0.75, *b*=0.5 and *b*=0.25 (Fig. 3). The calculation of l_{opt} was repeated for these four different positions of *CR*, assuming no change in all other model input parameters within each age class.

In theory, a *CR* positioned near the centre of volume of the snout implies that the snout must rotate over a larger angle θ_T (when snout–prey distance *d* remains constant) compared with a snout in which the *CR* is located near its posterior end. However, rotating over a larger angle with a similar amount of work inherently implies a decrease of the realised torque. This means that a *CR* near the eye will require a lower torque than a *CR* located near the posterior end of the head for the mouth to travel a certain distance. To investigate the relationship between torque, snout length and *CR* position we calculate the torque *Q* with the formula:

$$Q = \frac{E}{\theta_T} \quad . \tag{11}$$

RESULTS

Scaling of head and snout dimensions

The increase in head length is negatively allometric with respect to snout length (Table 1), indicating faster growth of the snout relative to the head. Snout width and snout height both scale negatively allometrically relative to snout length (Table 1). Head width and head height scale negatively allometrically with snout length (Table 1).

Centre of head rotation

The distance *R* between the centre of head rotation (*CR*) and the middle of the head volume scales negatively allometrically relative to head length (Table 1). The distance *r* between *CR* and the middle of the snout volume also shows a negatively allometric relation with snout length (Table 1). These results indicate that as the snout and the head length increase, the relative position of *CR* changes as well. The length of *R* and *r* relative to snout length changes from 0.60 and 0.61, respectively, for juveniles aged less than a week to 0.48 and 0.28, respectively, for adults. During growth, the position of *CR* changes in the anterior direction relative to the snout and head (Fig. 4). Furthermore, the slope of the log–log regression of total moment of inertia on snout length is 4.53±0.02 (Table 1), which is significantly lower than that predicted by isometry (slope=5).

Kinematics of head rotation

The magnitude of head rotation decreases during ontogeny. More specifically, the maximum head rotation in the earth-bound frame in the age classes less than 1 week, 1 week, 2 weeks, 3 weeks and adult is 44±2, 43±3, 37.7±1.7, 33.3±1.3 and 25±3 deg, respectively (mean ± s.e.m.) (Fig. 5A; Table 2). This decrease in head rotation is significant for the data of juveniles and adult combined, as well as within the juvenile data (Table 3). Additionally, smaller seahorses reach maximal head rotation earlier. The time to peak head rotation increases from 3.3±0.3, 3.11±0.17, 3.36±0.18 and 3.78±0.18 ms in the juveniles of less than 1 week, 1 week, 2 weeks, 3 weeks, respectively, to 6.4±0.9 ms in adults (Fig. 5A; Table 2). The increase in time to peak head rotation is also significant for the data of juveniles and adult combined as well as within the juvenile data (Table 3).

The larger head rotation combined with the shorter reach time results in higher angular velocities in smaller seahorses. More specifically, the maximal angular velocity of head rotation is 32.5±1.5, 33±4, 26.5±1.2, 21.9±1.4 and 15.3±1.2 10 deg s^{-1} for the juvenile age classes and adults, respectively (Fig. 5B and Table 2). This decrease of angular velocity is again significant in the data of juveniles and adults combined and within the juveniles (Table 3). The time to peak angular velocity of head rotation ranges from

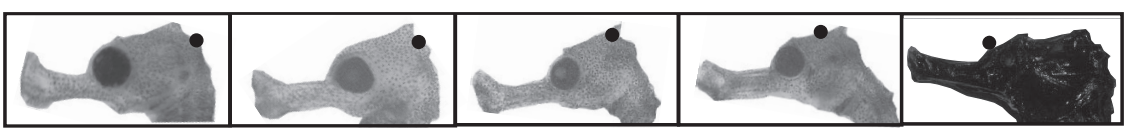

Fig. 4. Illustrations of the position of the centre of head rotation (*CR*) for the age classes (from left to right) <1 week, 1 week, 2 weeks, 3 weeks and adult.

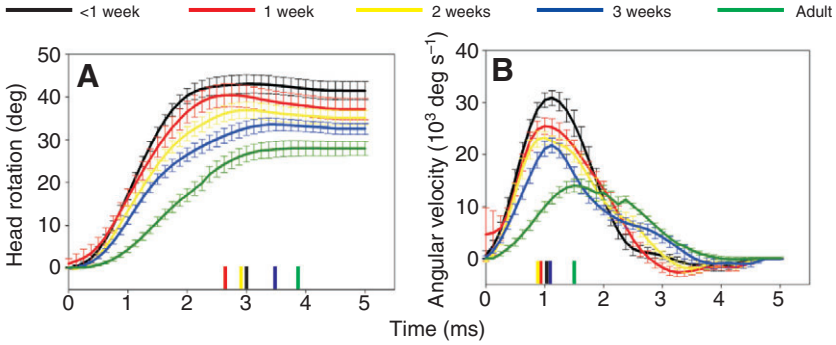

Fig. 5. The time profiles of the head rotation (A) and angular velocity (B) in each age class. Values are means ± s.e.m. The colour-coded vertical lines at the bottom of each graph indicate the time at which the profile with the same colour reaches its maximum. For details, see Table 2.

1.35±0.06, 1.32±0.08, 1.30±0.07, 1.40±0.05 ms in juveniles to 2.57±0.12 ms in adults (Fig. 5B and Table 2). In the data of juveniles and adults combined, the slope of the regression line shows a significant increase of angular velocity (Table 3). However, no clear relationship was found for the time to maximum angular velocity in the juvenile data (Table 3).

Optimal snout length

The results of the paired *t*-tests show that the optimal snout length is significantly longer than the measured snout length in each juvenile age class (Table 4). In the adults, however, there is no significant difference between the optimal snout length and the measured snout length (Table 4).

We also determined the range of snout lengths for which the model predicts a less than 5% increase in the time to reach the prey compared with the optimum reach time. All measured snout lengths of the juveniles are situated between the lower and upper limit of snout lengths set by this 5% increase of the minimal reach time (Table 5).

Effect of the centre of rotation position on optimal snout length

Moment of inertia

The total moment of inertia increases with increasing snout length. For example, in a juvenile less than 1 week old the total moment of inertia with respect to the centre of head rotation, obtained through the video recordings, is 0.94×10^{-12} kg m^2 for a snout length of 100% (i.e. the measured snout length). Doubling the snout length increases the moment of inertia relative to the same *CR* by 3.54 times. With a *CR* located at the posterior end of the snout, the total moment of inertia increases more rapidly with increasing snout length compared with a *CR* located more anteriorly and therefore closer to the centre of mass (Fig. 6).

Reach time

There is a clear difference between the juveniles and the adults in the effect of *CR* position on the time for the mouth to reach the prey. In the juveniles the combination of the real *b*, which is located near the posterior end of the snout, with the measured snout length is nearly optimal to minimise the reach time (t_{min}=2.75 ms for *b*=1 and a snout length of 100%). In adults, by contrast, the model predicts that the prey is reached faster with the combination of a *CR* located at the posterior end of the snout and a much shorter snout (t_{min}=2.91 ms for *b*=1 and a snout length of 38%; Fig. 6).

Required torque

According to the model, newborn seahorses show a *CR* for which a relatively high torque is required (to convert an amount of elastic energy into head rotation). Unlike juveniles, the adults display a *CR* for which relatively low torque is required (Fig. 6).

DISCUSSION

The main goal of this study was to test whether the snout length in seahorses is optimised to reach the prey as fast as possible for different ontogenetic stages. A recent mathematical model (de Lussanet and Muller, 2007) allowed us to calculate the theoretical optimal snout lengths, which were then compared with the actually measured snout lengths. Our results showed that the measured snout length in each juvenile age class (less than 1 week, 1, 2 and 3 weeks) was slightly shorter than the optimal snout length predicted by the model (Table 4). However, this small deviation from the predicted

Table 2. The results of the kinematic analysis of head rotation in the five age classes

Head rotation	<1 week (*N*=10)	1 week (*N*=13)	2 weeks (*N*=13)	3 weeks (*N*=14)	Adult (*N*=12)	
Maximum rotation (deg)		44±2	43±3	37.7±1.7	33.3±1.3	25±3
Time to maximum rotation (ms)		3.3±0.3	3.11±0.17	3.36±0.18	3.78±0.18	6.4±0.9
Maximum angular velocity ($\times10^3$ deg s^{-1})		32.5±1.5	33±4	26.5±1.2	21.9±1.4	15.3±1.2
Time to maximum angular velocity (ms)		1.35±0.06	1.32±0.08	1.30±0.07	1.40±0.05	2.57±0.12

Values are means ± s.e.m.

Table 3. Results of the log-transformed maximum head rotation, maximum angular velocity and their time to peak regressed to log head length for the juvenile and adult data and for the juvenile data without the adults

	Data of juveniles and adults (*N*=62)				Data of juveniles without adults (*N*=50)			
Head rotation	Slope	s.e.m.	R^2	*P*	Slope	s.e.m.	R^2	*P*
Maximum rotation	–0.21	0.03	0.38	<0.0001	–0.44	0.15	0.15	0.005
Time to maximum rotation	0.22	0.03	0.40	<0.0001	0.44	0.16	0.13	0.008
Maximum angular velocity	–0.25	0.03	0.48	<0.0001	–0.73	0.20	0.21	0.0009
Time to maximum angular velocity	0.26	0.03	0.51	<0.0001	0.02	0.22	<0.0005	0.92

Table 4. The statistical comparison between the measured snout length and the predicted, optimal snout length

Age	l (mm)	l_{opt} (mm)	t	d.f.	P
<1 week	2.16±0.01	2.51±0.02	–16.22	19	<0.0001
1 week	2.30±0.03	2.54±0.03	–12.69	19	<0.0001
2 weeks	3.08±0.07	3.35±0.13	–4.12	10	<0.0001
3 weeks	3.23±0.10	3.53±0.08	–5.33	14	<0.0001
Adult	19.35±0.44	19.22±0.52	0.71	9	0.50

Values are means ± s.e.m.
l, snout length; l_{opt}, optimal snout length; d.f., degrees of freedom.

optimum snout length corresponded to a difference of less than 1% from the shortest time to reach the prey that was predicted by the model if the snout length was perfectly optimised for this function (Table 5). Therefore, we must conclude that, similarly to adults, for which no statistical difference was found between the predicted and measured snout length (Table 4), the snout length in juveniles can also be considered as optimised to reach the prey as fast as possible.

Interestingly, the model predicts that the length of the snout can vary over a certain range (Table 5) around the optimum without a drastic decrease in head rotation performance. More specifically, there would only be a relatively small difference in minimal reach time (approximately +5%) if the snout was 50% longer than the actual snout observed in our study species (Table 5; Fig. 6). However, shortening the snout from the optimum results in a relatively stronger increase in reach time compared to lengthening (17% and 32% in snout length causes +5% in reach time for the youngest age class and adults, respectively). Despite this relatively limited effect of differences in snout length on head rotation performance, our results on *H. reidi* as well as a large number of other adult syngnathid species (de Lussanet and Muller, 2007) showed a remarkably close fit in snout length with the calculated optimum snout length. These findings suggest that there could be a relatively high selective pressure on snout length as a means of minimising prey reach time.

Given this relatively broad range of nearly optimal snout lengths (Table 5), one could argue that fishes that are not specialised pivot feeders may also fall within this near-optimal range. In contrast to pivot-feeding fish, other suction feeders use neurocranium rotation to increase the gape and expand the buccal cavity (Lauder, 1985; Van Wassenbergh et al., 2004; Gibb and Ferry-Graham, 2005) and thus do not decrease the predator–prey distance as in pivot feeders. However, because general suction feeding fishes are not adapted for pivot feeding, we would expect to find a poor match between the observed morphology and the predictions of the pivot-feeding model (de Lussanet and Muller, 2007). Indeed, when applying this model to a dorsoventral flattened catfish *Clarias gariepinus* and a lateral flattened sunfish *Lepomis gibbosus* (assuming that the region anterior to the eye represents the snout and the centre of rotation is identified as the joint between the supra-cleithrum and the post-temporal bones), the optimal snout length of the catfish and the sunfish for pivot feeding would be, respectively, approximately three and two times shorter than the measured length. This clearly shows that different optimisation criteria apply to the head morphology of pivot feeders *versus* non-pivot feeders.

According to Hernandez (Hernandez, 2000) the water flow regime could greatly affect the scaling of prey-capture kinematics. However, the model we used to calculate optimal snout lengths (de Lussanet and Muller, 2007) does not account for the effects of Reynolds number. Perhaps the small deviation between measured and predicted snout length in the juveniles is a result of the more viscous flow regime in which the juveniles live. To estimate the effect of the more viscous environment on the calculations of the optimal snout length, we increased the added mass around the rotating seahorse head as an approximating mimic of the increased volume of the boundary layer around the moving head. These simulations showed no effect on the model's output, suggesting that the difference in flow regime is probably not an important factor of influence on the optimal snout length in pivot feeders.

Another simplification in the model of de Lussanet and Muller (de Lussanet and Muller, 2007) is the assumption that the position of the centre of rotation (*CR*) of the species studied is equal to that of *Syngnatus acus*. This assumption should be used with caution as our analysis shows that the position of *CR* changes during ontogeny (Fig. 4), thereby affecting the results of the model (Fig. 6). For instance, in juveniles less than 1 week old the position of *CR* is located at the posterior end of the head, near the articulation of the head with the vertebral column (Fig. 4). When the snout of the juveniles grows longer, *CR* appears to shift in the direction of the snout tip, and in adults *CR* is located just above the eye (Fig. 4). Since the *CR* position inevitably has important effects on the dynamics of head rotation, this needs further examination.

We explored the consequences of this change in position of *CR* by calculating the total moment of inertia relative to four discrete positions of *CR* for different snout lengths in each age class (Fig. 6). Additionally we calculated the minimal reach time for each snout length at the four different positions of *CR* (Fig. 6). Our findings suggest that moving *CR* influences two aspects of pivot feeding.

Table 5. The results of the minimal reach time of the measured and predicted snout length, and upper and lower limits of optimal snout length for a 5% increase in prey reach time in each age class

Age	t_{min} for l (ms)	t_{min} for l_{opt} (ms)	l_{opt} (mm)	Upper limit of l_{opt} for t_{min} + 5% (mm)	Lower limit of l_{opt} for t_{min} + 5% (mm)
<1 week	2.77±0.05	2.75±0.03	2.51±0.02	1.79±0.02	3.64±0.02
1 week	3.06±0.02	3.04±0.04	2.54±0.03	1.74±0.04	3.74±0.04
2 weeks	3.15±0.08	3.14±0.11	3.35±0.13	2.45±0.08	4.57±0.08
3 weeks	3.24±0.09	3.23±0.10	3.53±0.08	2.85±0.09	5.32±0.09
Adult	5.89±0.23	5.89±0.25	19.22±0.52	13.10±0.41	27.62±0.42

Values are means ± s.e.m.
t_{min}, minimal reach time; l, snout length; l_{opt}, optimal snout length.

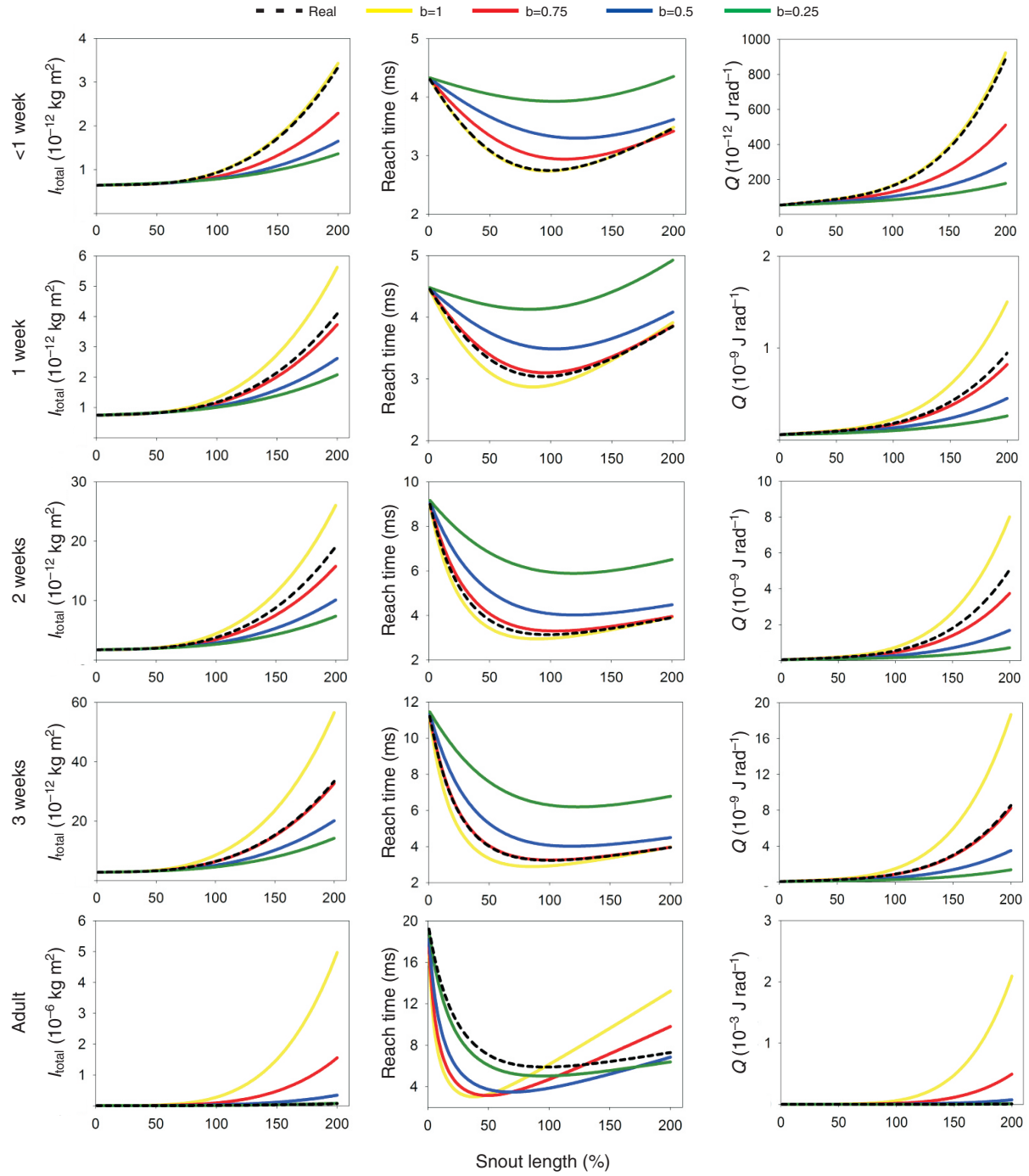

Fig. 6. An overview of the total moment of inertia I_{total} of the head and the snout (left column), the minimal reach time (middle column) and the required torque (Q; right column) for four different positions of the centre of rotation with increasing snout length for each age class. The four different positions of the centre of rotation are shown in Fig. 3. The simulation in which the measured distance of the centre of rotation is used, is represented by the black dashed line.

(1) decreasing the distance between *CR* and the middle of the snout decreases the total moment of inertia of the head and snout. This seems desirable, especially for individuals that are relatively large. (2) Decreasing the distance of *CR* to the middle of the snout increases the minimal reach time needed to bridge a certain distance, which probably decreases an individual's chances of prey capture. Consequently, a short snout with a large distance from the *CR* to the middle of the snout seems the most preferable situation: the total moment of inertia is nearly the same as for the same snout length with *CR* near the eye, and the animal has the shortest minimal reach time (Fig. 6). However, for rotations around a more posterior positioned *CR*, the animal must rotate its head over a relatively small angle to cover a given prey distance compared with an animal with the same snout length but with the *CR* located near the eye. In the latter case higher velocities will be reached, because of a lower torque (when energy input, *E*, is constant; Fig. 6). These results suggest that as the seahorse's snout length increases, it is preferable to have a *CR* close to the middle of the snout to reduce the moment

of inertia and the torque required to rotate the head, which is confirmed by our data (Fig. 4). The downside of this phenomenon is that the potential minimal reach time increases as the angle over which the head needs to be rotated increases with constant prey–snout distance.

Although snout length appears to be optimised for head rotation during ontogeny, the observed allometry of the head and snout during ontogeny may still have important effects on head rotation kinematics. Indeed, as seahorses get larger, their snout grows relatively faster than their head and also becomes relatively more slender, while head width and head height decrease relative to head length. The consequences of this shape change during growth for feeding performance may be significant, as an increase in relative snout length will decrease the angle over which the head is rotated during pivot feeding if prey position with respect to the snout tip remains identical. Our kinematic data support this and show that the maximal head rotation decreases from 44 deg in juveniles less than 1 week old to approximately 35 deg in juveniles 3 weeks of age and finally to 25 deg for adult *H. reidi* (Fig. 5A). As the head rotation angle decreases with increasing snout length, the time at which peak head rotation is achieved increases as well (Fig. 5A). As a result, the angular velocity of head rotation decreases in growing seahorses. The angular velocity of a juvenile of less than 1 week old is two times higher than that in adults, allowing them to reach the prey in times similar to or less than those observed for adults (Fig. 5B). The decrease in velocity during growth might be explained by our observation that the moment of inertia scales with $L^{4.53}$. This means that the rotational inertia most likely increases more rapidly than the available muscle moment in case of isometric growth (M=rF; r~L, F~L^2, thus M~L^3). Note that if the angular velocity is to remain constant, the cross-sectional area of the muscles must scale with $L^{3.53}$. Consequently, snout allometry indeed seems to be reflected in head rotation kinematics.

Despite the fact that both the juvenile and adult snout lengths are optimised to reach the prey as fast as possible, we observed that the feeding success in juveniles is relatively low compared with adults. The reason for this is currently unclear. Previous studies on pivot feeding in adult syngnathids showed that the kinematics of pivot feeding are relatively stereotypical (Muller, 1987; Bergert and Wainwright, 1997; Colson et al., 1998; de Lussanet and Muller, 2007; Van Wassenbergh et al., 2008; Roos et al., 2009a), but this is also the case for juveniles (Van Wassenbergh et al., 2009). Moreover, all muscles, ligaments and tendons involved in pivot feeding appear to be present in early juveniles (Van Wassenbergh et al., 2009; Leysen et al., 2010). Perhaps some unidentified developmental constraints exist which may explain the low prey capture success in juveniles.

A possible developmental constraint on feeding success in juvenile seahorses may be related to the position of the centre of rotation (*CR*) of the head and the potential effects of this on visual performance during feeding. Seahorses are visual predators (James and Heck, 1994; Curtis and Vincent, 2005; Mosk et al., 2007) feeding on small crustaceans (Kanou and Kohno, 2001; Teixeira and Musick, 2001; Woods, 2002; Kitsos et al., 2008). It could be important for the seahorse to maintain focus on the prey during head rotation to kinematically fine-tune the final stages of suction feeding. A *CR* located near the eye seems advantageous in this respect since this causes only little movement of the eye, which could result in sharp vision even during the fast rotation of the head. We observed that the adult seahorses focus their eyes in the direction of the prey at all time during the feeding strike (personal observation). In juveniles, however, *CR* is located almost half a snout length from the eye. Therefore the eye undergoes a large translation and rotation, which may result in blurred vision during the feeding strike. Although this could explain the relatively low prey capture success observed for juveniles, this idea will remain speculative as long as the nature and importance of visual feedback during pivot feeding is poorly understood.

CONCLUSION

Our data show that the relatively broad snout in newborn juveniles is optimised in length to reach the prey as fast as possible. Despite the fact that the measured snout length in juveniles is slightly shorter than the predicted snout length, the time to reach the prey for the snout lengths measured here is negligibly higher than the minimal reach time of the predicted snout lengths. When the snout becomes relatively narrower during growth, snout lengthening can also be explained as an optimisation for pivot feeding. This snout lengthening probably causes the observed decrease of the angle over which the head needs to be rotated during ontogeny. Additionally, the centre of head rotation (*CR*) has shifted towards the eye region, which decreases the moment of inertia and the torque required for rotating the head, and could improve potential visual feedback control during prey capture. However, these advantages of shifting *CR* forward trade off with a slight increase in the minimal prey reach time. Therefore, the complex relationship between snout length, *CR* position, and optimal reach time can be important determinants of feeding performance during ontogeny of syngnathid fish. The observed optimal snout length in juveniles right after being expelled from the male's brood pouch may imply that the early stages of ontogeny are subjected to strong selection (Carrier, 1996; Herrel and Gibb, 2006) and that the juveniles need similar high feeding performance (i.e. reaching the prey in minimal time) as that of adults to survive.

LIST OF SYMBOLS AND ABBREVIATIONS

b	the distance between *CR* and the midpoint of the snout along the snout length axis, divided by the distance between the most posterior point on the head and *CR* along the same axis
CR	centre of head rotation in the earth-bound frame of reference
d	distance between the snout tip and the prey
E	rotational kinetic energy
f	distance between the snout tip and the centre of rotation
h	snout height
H	head height
I_{head}	moment of inertia of the head relative to the centre of rotation
I_{snout}	moment of inertia of the snout relative to the centre of rotation
I_{total}	total moment of inertia of head and snout relative to the centre of rotation
l	snout length
l_{opt}	optimal snout length predicted by the model
L	head length
Q	torque
r	distance between the centre of rotation and the middle of the snout volume
R	distance between the centre of rotation and the middle of the head volume
t	reach time
t_{min}	minimal reach time predicted by the model
w	snout width
W	head width
α_{head}	added mass coefficient of the head
α_{snout}	added mass coefficient of the snout
ρ	density of seawater
$\bar{\theta}_T$	average maximal angular velocity of head rotation
θ_T	head rotation

ACKNOWLEDGEMENTS

G.R. is funded by a PhD grant from the Institute for the Promotion of Innovation through Science and Technology in Flanders (IWT-Vlaanderen). S.V.W. is a postdoctoral fellow of the Fund for Scientific Research, Flanders (FWO-Vl), supported by FWO-Vl grant G 053907. The authors thank David Vuylsteke, Joachim Christiaens and Heleen Leysen for taking care of the juvenile seahorses, and three anonymous reviewers for their helpful comments on the manuscript.

REFERENCES

Bergert, B. A. and Wainwright, P. C. (1997). Morphology and kinematics of prey capture in the syngnathid fishes *Hippocampus erectus* and *Syngnathus floridae*. *Mar. Biol.* **127**, 563-570.

Carrier, D. R. (1995). Ontogeny of jumping performance in the black tailed jack rabbit (*Lepus californicus*). *Zoology* **94**, 309-313.

Carrier, D. R. (1996). Ontogenetic limits on locomotor performance. *Physiol. Zool.* **69**, 467-488.

Choo, C. K. and Liew, H. C. (2006). Morphological development and allometric growth patterns in the juvenile seahorse *Hippocampus kuda* Bleeker. *J. Fish. Biol.* **69**, 426-445.

Colson, D. J., Patek, S. N., Brainerd, E. L. and Lewis, S. M. (1998). Sound production during feeding in *Hippocampus* seahorses (Syngnathidae). *Environ. Biol. Fish.* **51**, 221-229.

Curtis, J. M. R. and Vincent, A. C. J. (2005). Distribution of sympatric seahorse species along a gradient of habitat complexity in a seagrass-dominated community. *Mar. Ecol. Prog. Ser.* **291**, 81-91.

Daniel, T. L. (1984). Unsteady aspects of aquatic locomotion. *Am. Zool.* **24**, 121-134.

de Lussanet, M. H. E. and Muller, M. (2007). The smaller your mouth, the longer your snout: predicting the snout length of *Syngnathus acus*, *Centriscus scutatus* and other pipette feeders. *J. R. Soc. Interface* **4**, 561-573.

Drost, M. R. and van den Boogaart, J. G. M. (1986). A simple method for measuring the changing volume of small biological objects, illustrated by studies of suction feeding by fish larvae and of shrinkage due to histological fixation. *J. Zool. Lond.* **209**, 239-249.

Forsgren, K. L. and Lowe, C. G. (2006). The life history of weedy seadragons, *Phyllopteryx taeniolatus* (Teleostei: Syngnathidae). *Mar. Freshwater Res.* **57**, 313-322.

Gibb, A. C. (1997). Do flatfish feed like other fishes? A comparative study of percomorph prey-capture kinematics. *J. Exp. Biol.* **200**, 2841-2859.

Gibb, A. C. and Ferry-Graham, L. A. (2005). Cranial movements during suction feeding in teleost fishes: are they modified to enhance suction production? *Zoology* **108**, 141-153.

Gibb, A. C., Swanson, B. O., Wesp, H., Landels, C. and Liu, C. (2006). Development of the escape response in teleost fishes: do ontogenetic changes enable improved performance? *Physiol. Biochem. Zool.* **79**, 7-19.

Hernandez, L. P. (2000). Intraspecific scaling of feeding mechanics in an ontogenetic series of zebrafish, *Danio rerio*. *J. Exp. Biol.* **203**, 3033-3043.

Herrel, A. and Gibb, A. C. (2006). Ontogeny of performance in vertebrates. *Physiol. Biochem. Zool.* **79**, 1-6.

Herrel, A. and O'Reilly, J. C. (2006). Ontogenetic scaling of bite force in lizards and turtles. *Physiol. Biochem. Zool.* **79**, 31-42.

Holzman, R., Day, S. W. and Wainwright, P. C. (2007). Timing is everything: coordination of strike kinematics affects the force exerted by suction feeding fish on attached prey. *J. Exp. Biol.* **210**, 3328-3336.

Holzman, R., Day, S. W., Mehta, R. S. and Wainwright, P. C. (2008). Jaw protrusion enhances forces exerted on prey by suction feeding fishes. *J. R. Soc. Interface* **5**, 1445-1457.

James, P. L. and Heck, K. L. J. (1994). The effects of habitat complexity and light intensity on ambush predation within a simulated seagrass habitat. *J. Exp. Mar. Biol. Ecol.* **176**, 187-200.

Kanou, K. and Kohno, H. (2001). Early life history of a seahorse, *Hippocampus mohnikei*, in Tokyo Bay, Japan. *Ichthyol. Res.* **48**, 361-368.

Kendrick, A. J. and Hyndes, G. A. (2005). Variations in the dietary compositions of morphologically diverse syngnathid fishes. *Environ. Biol. Fishes* **72**, 415-427.

Kitsos, M.-S., Tzomos, T., Anagnostopoulou, L. and Koukouras, A. (2008). Diet composition of the seahorses, *Hippocampus guttulatus* Cuvier, 1829 and *Hippocampus hippocampus* (L., 1758) (Teleostei, Syngnathidae) in the Aegean Sea. *J. Fish Biol.* **72**, 1259-1267.

Lauder, G. V. (1985). Aquatic feeding in lower vertebrates. In *Functional Vertebrate Morphology* (ed. M. Hildebrand, D. M. Bramble, K. F. Liem and D. B. Wake), pp. 210-299. Campridge, MA: Harvard University Press.

Leysen, H., Jouk, P., Brunain, M., Christiaens, J. and Adriaens, D. (2010). Cranial architecture of tube-snouted gasterosteiformes (*Syngnathus rostellatus* and *Hippocampus capensis*). *J. Morphol.* **271**, 255-270.

Lourie, S. A. and Randall, J. E. (2003). A new pygmy seahorse, *Hippocampus denise* (Teleostei: Syngnathidae), from the Indo-Pacific. *Zool. Stud.* **42**, 284-291.

Lourie, S. A., Vincent, A. C. J. and Hall, H. J. (1999). *Seahorses: an Identification Guide to the World's Species and Their Conservation.* London: Project Seahorse.

Moon, B. R. and Tullis, A. (2006). The ontogeny of contractile performance and metabolic capacity in a high-frequency muscle. *Physiol. Biochem. Zool.* **79**, 20-30.

Mosk, V., Thomas, N., Hart, N. S., Partridge, J. C., Beazley, L. D. and Shand, J. (2007). Spectral sensitivities of the seahorses *Hippocampus subelongatus* and *Hippocampus barbouri* and the pipefish *Stigmatopora argus*. *Visual Neurosci.* **24**, 345-354.

Muller, M. (1987). Optimization principles applied to the mechanism of neurcranium levation and mouth bottom depression in bony fishes (Halecostomi). *J. Theor. Biol.* **126**, 343-368.

Muller, M. and Osse, J. W. M. (1984). Hydrodynamics of suction feeding in fish. *Trans. Zool. Soc. Lond.* **37**, 51-135.

Roos, G., Leysen, H., Van Wassenbergh, S., Herrel, A., Jacobs, P., Dierick, M., Aerts, P. and Adriaens, D. (2009a). Linking morphology and motion: a test of a four-bar mechanism in seahorses. *Physiol. Biochem. Zool.* **82**, 7-19.

Roos, G., Van Wassenbergh, S., Herrel, A. and Aerts, P. (2009b). Kinematics of suction feeding in the seahorse *Hippocampus reidi*. *J. Exp. Biol.* **212**, 3490-3498.

Sokal, R. R. and Rohlf, F. J. (1995). *Biometry: the Principles and Practice in Biological Research*. New York, NY: Freeman.

Tchernavin, V. V. (1953). *Feeding Mechanisms of a Deep Sea Fish Chauliodus Sloani Schneider*. London, UK: The Trustees of the British Museum.

Teixeira, R. L. and Musick, J. A. (2001). Reproduction and food habits of the lined seahorse, *Hippocampus erectus* (Teleostei: Syngnathidae) of Chesapeake Bay, Virginia. *Rev. Brasil. Biol.* **61**, 79-90.

Van Wassenbergh, S., Herrel, A., Adriaens, D. and Aerts, P. (2004). Effects of jaw adductor hypertrophy on buccal expansions during feeding of air breathing catfishes (Teleostei, Clariidae). *Zoomorphology* **123**, 81-93.

Van Wassenbergh, S., Strother, J. A., Flammang, B. E., Ferry-Graham, L. A. and Aerts, P. (2008). Extremely fast prey capture in pipefish is powered by elastic recoil. *J. R. Soc. Interface* **5**, 285-296.

Van Wassenbergh, S., Roos, G., Genbrugge, A., Leysen, H., Aerts, P., Adriaens, D. and Herrel, A. (2009). Suction is kids play: extremely fast suction in newborn seahorses. *Biol. Lett.* **5**, 200-203.

Wainwright, P. C. and Day, S. W. (2007). The forces exerted by aquatic suction feeders on their prey. *J. R. Soc. Interface* **4**, 553-560.

Woods, C. M. C. (2002). Natural diet of the seahorse *Hippocampus abdominalis*. *New Zealand J. Mar. Fresh.* **36**, 655-660.